

# Ultra Memory-Efficient On-FPGA Training of Transformers via Tensor-Compressed Optimization

Jiayi Tian, Jinming Lu, Hai Li, Xiangwei Wang, Cong (Callie) Hao, Ian Young, *Fellow, IEEE*, Zheng Zhang

**Abstract**—Transformer models have achieved state-of-the-art performance across a wide range of machine learning tasks. There is growing interest in training transformers on resource-constrained edge devices due to considerations such as privacy, domain adaptation, and on-device scientific machine learning. However, the significant computational and memory demands required for transformer training often exceed the capabilities of an edge device. Leveraging low-rank tensor compression, this paper presents the first on-FPGA accelerator for end-to-end transformer training. On the algorithm side, we present a bi-directional contraction flow for tensorized transformer training, significantly reducing the computational FLOPS and intra-layer memory costs compared to existing tensor operations. On the hardware side, we store all highly compressed model parameters and gradient information on chip, creating an on-chip-memory-only framework for each stage in training. This reduces off-chip communication and minimizes latency and energy costs. Additionally, we implement custom computing kernels for each training stage and employ intra-layer parallelism and pipe-lining to further enhance run-time and memory efficiency. Through experiments on transformer models within 36.7 to 93.5 MB using FP-32 data formats on the ATIS dataset, our tensorized FPGA accelerator could conduct single-batch end-to-end training on the AMD Alevo U50 FPGA, with a memory budget of less than 6-MB BRAM and 22.5-MB URAM. Compared to uncompressed training on the NVIDIA RTX 3090 GPU, our on-FPGA training achieves a memory reduction of  $30\times$  to  $51\times$ . Our FPGA accelerator also achieves up to  $3.6\times$  less energy cost per epoch compared with tensor Transformer training on an NVIDIA RTX 3090 GPU. As an initial result, this work highlights the significant potential of low-rank tensor algebra in enabling large-scale training on edge devices.

**Index Terms**—Transformer Models, FPGA Accelerator, On-Device Training, Low-Rank Tensor Compression.

## I. INTRODUCTION

THERE has been growing interest in on-device training of machine learning models. In finance, healthcare, and smart homes, there have been increasing concerns about users' data privacy [1], [2]. This has driven federated learning [3], [4] on edge devices to train AI models end-to-end or incrementally based on local private data. In robotic and autonomous

systems, machine learning has shown great promise in high-dimensional safety verification and control [5]–[7], where the neural network needs to be trained again as the system dynamics or safety regions keep updated. Meanwhile, pre-trained AI model often suffers from performance degradation in practical deployment due to the uncertain environment and data distribution shift [8], necessitating on-device model adaptation. Due to the limited size, weight, and power budget, resource-constrained devices such as FPGA, microcontrollers, or embedded GPUs are often used for edge AI. In recent years, several edge training accelerators have been proposed for convolutional neural networks [9], [10], multilayer perceptron networks, or recurrent neural networks [11]–[13]. Most existing work focuses on on-device fine-tuning or transfer learning (rather than more challenging end-to-end training) due to the limited computing and memory budget.

Meanwhile, transformer models [14] have achieved state-of-the-art performance in numerous application domains, including (but not limited to) natural language processing [14], [15], computer vision [16], [17] and scientific simulation [18]. However, the substantial memory and computational burdens of transformers have posed new challenges for their training and deployment on resource-constrained devices. For instance, the model parameters of a medium-size transformer can easily exceed the memory capacity of an edge device (e.g. FPGA), making it nontrivial to perform inference and infeasible to perform training on an edge device. Recent works have investigated quantization [19]–[21], low-rank compression [22], [23], pruning [24], [25] and knowledge distillation [26] to reduce the cost of fine-tuning on GPU or inference on edge devices for transformer models. However, training transformers (especially from scratch) on resource-constrained devices remain a great challenge, due to two main factors:

- Firstly, it is hard to meet the memory requirement of transformer training. A transformer model can easily consume  $> 5\times$  more on-chip memory than the capacity of an FPGA. It is difficult to fill this memory gap even if sparse [27] or low-precision training [21], [28]–[30] methods are utilized. For example, ideal memory reduction (which is hard to achieve in practice) is limited to  $8\times$  even if ultra-low-precision 4-bit training [30] is used.
- Secondly, on-device training involves more computing tasks than on-device inference, such as backward propagation, gradient generation, and parameter update. This increases both the memory and computing burden on the edge devices. Furthermore, data dependency between forward and back propagations further complicates data communication, task

J. Tian, J. Lu and Z. Zhang are with Department of Electrical and Computer Engineering, University of California, Santa Barbara, CA 93106; H. Li and I. Young are with Intel Corporation, Hillsboro, OR 97124; X. Wang is with Department of Computer Science, North Carolina State University. He participated in this work when he was an exchange undergraduate student at UCSB; C. Hao is with School of Electrical and Computer Engineering, Georgia Institute of Technology, Atlanta, GA 30332. She participated in this work before Intel funded this project. (email: jiayi\_tian@ucsb.edu; jinminglu@ucsb.edu; hai.li@intel.com; xwang258@ncsu.edu; callie.hao@gatech.edu; ian.young@intel.com; zhengzhang@ece.ucsb.edu).

scheduling, and memory management.

In this paper, we use FPGA as a demonstration to investigate the end-to-end training of transformer models on edge devices that leverage low-rank tensor optimization. As a high-dimensional generalization of matrix decomposition [31], tensor decomposition can achieve much higher compression ratios in neural networks. This may provide a huge reduction in memory and computing costs, enabling on-device training of large AI models that were previously infeasible. Previous work has shown orders-of-magnitude model reduction by low-rank tensor decomposition in post-training compression [32]–[34] and motivated some memory-efficient inference hardware accelerator design [35]–[40]. Recent work has shown huge model compression through low-rank tensor-compressed training [41]–[43]. Some recent work has shown high accuracy of rank-adaptive tensor-compressed training [44]–[46], speedup over standard pre-training on transformers and large language models (LLM) via GPU optimization [44], as well as memory savings and communication reduction for LLM fine-tuning [23], [47], [48]. Using these algorithmic results, some previous work also developed tensor-compressed methods without backpropagation to train small neural networks on photonic platforms [37], [49]. However, current backpropagation-free training cannot handle transformer-size models due to its large gradient estimation error, and on-device transformer training from scratch remains an open problem.

To fill the research gap described above, this paper presents, for the first time, an FPGA accelerator for low-rank tensor-compressed transformer training *from scratch*. This research can be regarded as a proof-of-concept demonstration and a pathfinding effort toward future ASIC implementation. Using previous algorithmic research [44]–[46], this article presents the following novel contributions:

- We design an end-to-end tensor-compressed transformer training accelerator implemented on FPGA. Using tensor decomposition, transformer training becomes ultra memory-efficient, allowing end-to-end training of up to 93.5-MB model with an 28.4-MB SRAM memory budget [including less than 6-MB block RAM (BRAM) capacity].
- We present a novel bidirectional tensor contraction technique that significantly improves the computing and memory efficiency of tensor-compressed forward and backward propagation. This contraction flow surpasses the sequential computation flows employed in previous inference accelerators [39], [40]. In addition, we develop a comprehensive model for analyzing the computing and memory costs associated with various tensor decomposition formats and contraction orders.
- We optimize the parallel scheduling flow and develop an intrastage fine-grained pipelining strategy to enhance the trade-off between run-time and hardware cost. Additionally, we propose an on-chip memory management strategy to further improve the memory efficiency of our FPGA training accelerator.
- We implement the training method on an AMD Alveo U50 FPGA, evaluate hardware performance using the ATIS dataset [50] on a transformer model with various number

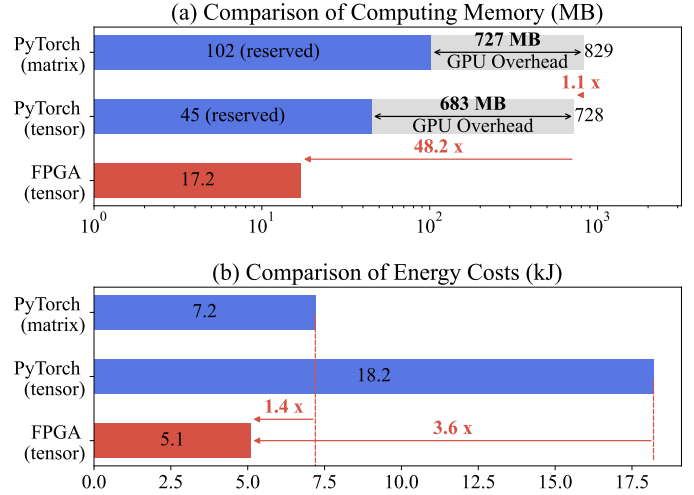


Fig. 1. Comparison of computing memory consumption (top) and energy costs (bottom) between PyTorch-based GPU training and our accelerator; blue bars represent reserved CUDA memory without additional overhead. The results are measured on the training task of a 2-encoder transformer.

of encoding blocks. Experimental results demonstrate that our FPGA accelerator can achieve  $3.6\times$  lower energy costs with  $48\times$  reduction in computing memory compared to uncompressed training using Pytorch on a Nvidia RTX 3090 GPU, as highlighted in Fig. 1.

As a preliminary study, this work has not used any pruning or quantization techniques, and there hardware resource is still under utilized. Therefore, the performance gain can be further improved in the future. However, the current initial study suffices to demonstrate the great potential of low-rank tensor computation to scale up training on edge devices.

## II. BACKGROUND

In this section, we introduce some necessary background related to our work.

### A. Transformer Models

A transformer model consists of a stack of encoder or decoder blocks. For discrimination tasks, one can use encoders only to process the input sequence and generate output representations. For generative tasks, decoders should be used to generate the output sequence step by step, using both the encoded input and its own previous output. A encoder block and a decoder block have the same structure, a self-attention layer, and a feed-forward network (FFN). Both encoder and decoder blocks include residual connections and layer normalization to stabilize training. The computation in one encoder block could be written sequentially as

$$\mathbf{Q} = \mathbf{W}_q \mathbf{X} + \mathbf{B}_q, \mathbf{K} = \mathbf{W}_k \mathbf{X} + \mathbf{B}_k, \mathbf{V} = \mathbf{W}_v \mathbf{X} + \mathbf{B}_v,$$

$$\text{Attention}(\mathbf{Q}, \mathbf{K}, \mathbf{V}) = \text{softmax}\left(\frac{\mathbf{Q}\mathbf{K}^T}{\sqrt{d_k}}\right)\mathbf{V},$$

$$\mathbf{Y}_{\text{attn}} = \text{LN}(\mathbf{W}_o \text{Attention}(\mathbf{Q}, \mathbf{K}, \mathbf{V}) + \mathbf{B}_o + \mathbf{X}),$$

$$\mathbf{Y}_{\text{ffn}} = \text{LN}(\mathbf{W}_2 \text{GELU}(\mathbf{W}_1 \mathbf{Y}_{\text{attn}} + \mathbf{B}_1) + \mathbf{B}_2 + \mathbf{Y}_{\text{attn}}).$$

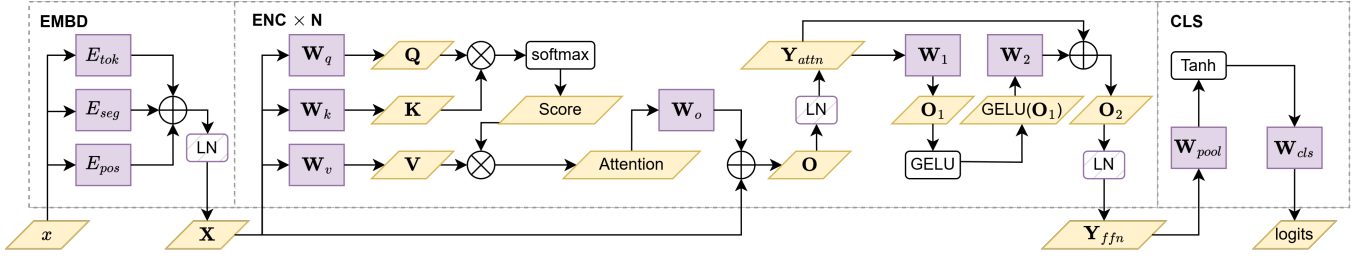


Fig. 2. Transformer structure for classification tasks. Inter-layer activation is represented using yellow blocks, embedding tables and linear layer weights are in purple blocks, and non-linear functions are in white blocks.

Here,  $\mathbf{X}$  is the input of an encoder;  $\mathbf{Y}_{\text{attn}}$  and  $\mathbf{Y}_{\text{ffn}}$  are the outputs of the attention layer and the feed-forward network, respectively;  $\mathbf{W}_q, \mathbf{W}_k, \mathbf{W}_v$  and  $\mathbf{W}_o$  are the weights in attention;  $\mathbf{Q}, \mathbf{K}$  and  $\mathbf{V}$  are the query, key, and value features, respectively;  $\mathbf{W}_1$  and  $\mathbf{W}_2$  are the weights in a feed-forward network; LN represents the layer normalization operation. The nonlinear functions in the attention layers and feed-forward networks are softmax and GELU, respectively.

An embedding layer converts discrete input tokens (e.g. words or subwords) to dense vectors that can capture semantic relationships and be processed by the attention mechanism. Firstly, positional embeddings  $E_{\text{pos}}$  are added to the input tokens to preserve their order, since the self-attention mechanism lacks built-in sequence understanding. Secondly, segment and token embeddings are required in natural language processing to process an input sequence. The token embedding  $E_{\text{tok}}$  converts words or subwords from a vocabulary into continuous vector representations. Segment embeddings  $E_{\text{seg}}$  differentiate tokens from different segments (e.g. sentences A and B) in tasks such as sentence-pair classification. The embedding layer of a transformer can be written as

$$z_i = E_{\text{tok}}(x_i) + E_{\text{pos}}(i) + E_{\text{seg}}(p_i), \quad (1)$$

where  $i$  is the position of the token  $x_i$  in the sequence.

Additionally, for classification tasks, a classifier (composed of linear layers followed by an activation function) should be applied to the final hidden representation of the [CLS] token for discrimination tasks.

The general structure of a typical transformer model for classification tasks is shown in Fig. 2.

### B. Tensor Decomposition and Contraction

Tensors are a high-dimensional generalization of matrices and vectors. A generic  $d$ -way could be represented as  $\mathcal{A} \in \mathbb{R}^{n_1 \times \dots \times n_d}$ , where  $n_k$  is the size of the mode (or dimension)  $k$ . The  $(i_1, i_2, \dots, i_d)$ -th element of  $\mathcal{A}$  is written as  $a_{i_1, i_2, \dots, i_d}$  or  $\mathcal{A}(i_1, i_2, \dots, i_d)$ . One can also use graphs to represent tensor operators. Specifically, a  $d$ -way tensor is denoted by a node with  $d$  edges. If two nodes are connected by an edge, then a tensor contraction happens between them, and the connected mode will diminish. Consider, for example,  $\mathcal{A} \in \mathbb{R}^{n_1 \times \dots \times n_d}$  and  $\mathcal{B} \in \mathbb{R}^{m_1 \times \dots \times m_l}$ . Assume that  $n_s = m_t$ , the tensor contraction of these two tensors could be formulated as

$$\mathcal{C} = \mathcal{A} \times_s^t \mathcal{B}. \quad (2)$$

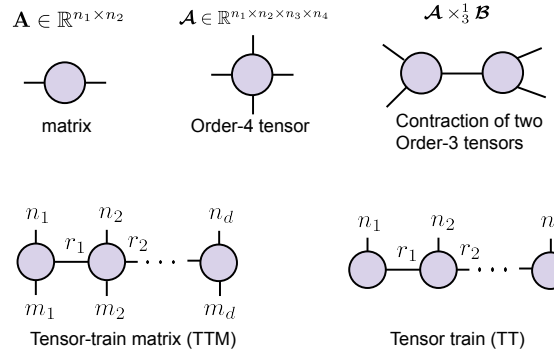


Fig. 3. Tensor graph representation for tensors, tensor contraction, and tensor networks for TTM and TT decomposition.

Tensor  $\mathcal{C} \in \mathbb{R}^{n_1 \times \dots \times n_{s-1} \times n_{s+1} \times \dots \times n_d \times m_1 \times \dots \times m_{t-1} \times m_{t+1} \times \dots \times m_l}$  has  $d+l-2$  modes, and each element of  $\mathcal{C}$  is

$$c_{i_1, \dots, i_{s-1}, i_{s+1}, \dots, i_d, j_1, \dots, j_{t-1}, j_{t+1}, \dots, j_l} = \sum_{i_s=1}^{m_s} a_{i_1, \dots, i_s, \dots, i_d} b_{j_1, \dots, j_{t-1}, i_s, \dots, j_l} \quad (3)$$

The contraction operations of multiple tensors can be represented as a tensor network with many nodes and edges. The number of free edges in a tensor network decides the final shape and size of the resulting tensor.

It is expensive to store and compute high-dimensional tensors directly. Fortunately, practical tensors can often be compressed by low-rank tensor decompositions [31]. We mainly use the tensor-train (TT) decomposition [51] and its variant tensor-train-matrix (TTM) decomposition for compressed training. TT decomposes a tensor  $\mathcal{A} \in \mathbb{R}^{n_1 \times \dots \times n_d}$  as

$$\mathcal{A} = \mathcal{G}_1 \times_3^1 \mathcal{G}_2 \times_3^1 \dots \mathcal{G}_d, \quad (4)$$

where  $\mathcal{G}_k \in \mathbb{R}^{r_{k-1} \times n_k \times r_k}$  is a TT factor,  $(r_0, r_1, \dots, r_d)$  is called TT rank, and  $r_0 = r_d = 1$ . TTM decomposes an order- $2d$  tensor  $\mathcal{W} \in \mathbb{R}^{n_1 \times \dots \times n_d \times m_1 \times \dots \times m_d}$  as

$$\mathcal{W} = \mathcal{F}_1 \times_4^1 \mathcal{F}_2 \times_4^1 \dots \mathcal{F}_d, \quad (5)$$

where  $\mathcal{F}_k \in \mathbb{R}^{r_{k-1} \times n_k \times m_k \times r_k}$ , and  $r_0 = r_d = 1$ .

The graph representations for tensors, tensor contractions, and tensor networks for TTM and TT are shown in Fig. 3.

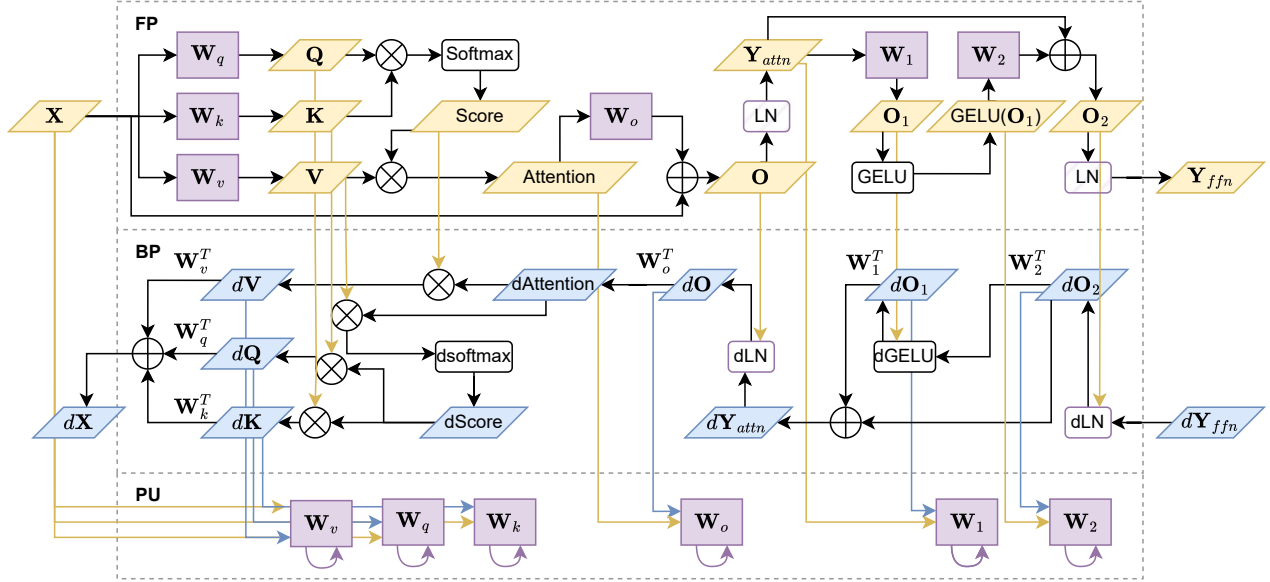


Fig. 4. Detailed training flow of one encoder block, including forward propagation (FP), backward propagation (BP), and model parameter update (PU). The yellow blocks represent activations, blue blocks represent activation gradients, purple blocks represent model parameters.

### C. Tensor-Compressed Neural Network

Tensor decomposition has been widely adopted to reduce the model size in various neural networks [41], [45], [46], [52]–[54]. Among the various low-rank tensor formats, TT and TTM are the most widely used due to their exceptional accuracy, orders of magnitude compression ratios, and straightforward data structures [22], [41], [44], [55], [56]. In this work, we mainly use TT to compress the weight matrices and TTM to compress the embedding table for efficient transformer training.

We consider the weight matrix  $\mathbf{W} \in \mathbb{R}^{M \times N}$  in a linear layer. Assume  $M = \prod_i m_i$  and  $N = \prod_i n_i$ , and we reshape the matrix  $\mathbf{W}$  into an order- $2d$  tensor  $\mathcal{W} \in \mathbb{R}^{m_1 \times \dots \times m_d \times n_1 \times \dots \times n_d}$ . With TT decomposition, we can represent  $\mathcal{W}$  with TT cores  $\{\mathcal{G}_k\}_{k=1}^{2d}$  as

$$\mathcal{W} = \mathcal{G}_1 \times_3^1 \dots \mathcal{G}_k \times_3^1 \dots \mathcal{G}_d \times_3^1 \dots \mathcal{G}_{d+k} \times_3^1 \mathcal{G}_{2d}, \quad (6)$$

Here  $\mathcal{G}_k \in \mathbb{R}^{r_{k-1} \times m_k \times r_k}$  when  $1 \leq k \leq d$  and  $\mathcal{G}_k \in \mathbb{R}^{r_{k-1} \times n_k \times r_k}$  when  $d+1 \leq k \leq 2d$ . The total number of variables in  $\mathcal{W}$  is reduced to  $\sum_{k=1}^d (r_{k-1} m_k r_k + r_{k-1} n_k r_{k+d})$  from  $\prod_{k=1}^d m_k n_k$ , which approximately achieves  $O(m^d n^d) \rightarrow O(d r^2 (m+n))$  memory reduction.

For the embedding table, we follow [43], [44] and use TTM to compress the vocab dictionary. We first reshape the token embedding layer  $\mathbf{E}_{\text{tok}} \in \mathbb{R}^{M \times N}$  to  $\mathcal{E}_{\text{tok}} \in \mathbb{R}^{m_1 \times n_1 \times \dots \times m_d \times n_d}$ , where  $M = \prod_i m_i$  and  $N = \prod_i n_i$ . We define the TTM representation for the token embedding layer as

$$\mathcal{E}_{\text{tok}} = \mathcal{F}_1 \times_4^1 \dots \mathcal{F}_k \times_4^1 \dots \mathcal{F}_d, \quad (7)$$

where  $\mathcal{F}_k \in \mathbb{R}^{r_{k-1} \times m_k \times n_k \times r_k}$ . TTM reduces the number of parameters from  $\prod_{k=1}^d m_k n_k$  to  $\sum_{k=1}^d (r_{k-1} m_k n_k r_k)$ , achieving  $O(m^{d-1} n^{d-1} / d r^2)$  memory reduction.

## III. TENSORIZED TRANSFORMER TRAINING

### A. Overall Training Framework

We consider the transformer in Fig. 2, which has one embedding layer,  $N$  encoder blocks and a task-specific classifier. The three embedding tables for token, position, and segment are compressed to TTM as done in [44]. All weight matrices (including those in the attention layers and feed-forward layers) of the encoder blocks are compressed to TT. The fully connected weight matrices in the classifier are also compressed to TT. The last task-specific linear layer for classification is kept uncompressed. In the training process, we use stochastic gradient descent (SGD) to solve the optimization problem

$$\min_{\theta} \mathcal{L}(\theta, \mathcal{D}), \quad (8)$$

where  $\mathcal{D}$  is the training dataset. Note that the training variables  $\theta$  include compression factors once a matrix is parameterized in a TT or TTM format. This differs from standard training where only large-scale 2-D matrices are trained.

**Training Process.** Our end-to-end tensorized transformer training includes three stages:

- 1) **Forward propagation (FP).** In a forward pass, the input tokens are fed into the embedding layer to generate hidden features, then the  $N$  encoders sequentially process the input features, and finally the classifier computes predictions and loss. The main computations, matrix-vector products, are replaced with low-rank tensor-network contractions. Since the original weight matrices are not recovered, a significant reduction in memory and FLOPS can be achieved.
- 2) **Backward propagation (BP).** The BP process first computes the gradients of the loss with respect to feature values according to a chain rule. After that, the gradient

$$\mathcal{G}'_{d+k}[i_{d+k}] = \sum_{i_1, \dots, i_d, j_1, \dots, j_{k-1}, j_{k+1}, \dots, j_d} (\mathcal{G}_{d+k-1}^T[j_{k-1}] \dots \mathcal{G}_1^T[i_1] y'_{i_1, \dots, i_d}) (x_{j_1, \dots, j_d} \mathcal{G}_{2d}^T[j_d] \dots \mathcal{G}_{d+k+1}^T[j_{k+1}]), \quad (9)$$

$$\mathcal{G}'_k[i_k] = \sum_{i_1, \dots, i_{k-1}, i_{k+1}, \dots, i_d, j_1, \dots, j_d} (\mathcal{G}_{k-1}^T[i_{k-1}] \dots \mathcal{G}_1^T[i_1] y'_{i_1, \dots, i_d}) (x_{j_1, \dots, j_d} \mathcal{G}_{2d}^T[j_d] \dots \mathcal{G}_{k+1}^T[i_{k+1}]), \quad \text{for } k \in [1, d] \quad (10)$$

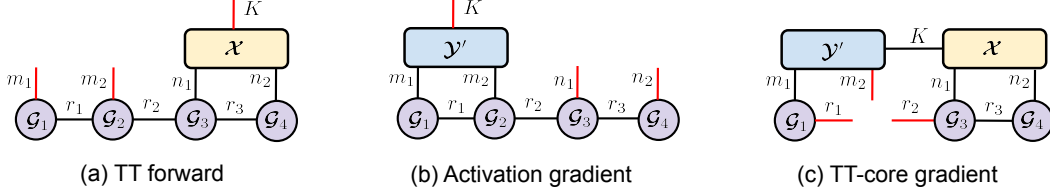


Fig. 5. Tensor graph representations for the TT-format (a) forward propagation, (b) gradient computation w.r.t. activations and (c) gradient computation w.r.t. a TT core (with  $\mathcal{G}_2$  as an example) of a linear layer. For simplicity, here we assume  $d = 2$  and that the matrix is fold to a tensor of order  $2d = 4$ . The red lines denote free edges of a tensor network, which indicate the dimension of the result tensor.

with respect to each TT factor is also computed via a tensor network contraction.

- 3) **Model parameter update (PU).** The model parameters are updated as  $\theta \leftarrow \theta - \alpha \theta'$ , where  $\alpha$  is a learning rate and  $\theta' = \frac{\partial \mathcal{L}}{\partial \theta}$  is the (stochastic) gradient. Since we use tensor-compressed training, updates are also performed on TT or TTM factors for compressed layers. For example, a TT core  $\mathcal{G}_k$  is updated as  $\mathcal{G}_k \leftarrow \mathcal{G}_k - \alpha \mathcal{G}'_k$  in each iteration.

Fig. 4 shows the detailed training flow that includes all three training phases of the encoder. In the following two subsections, we present the key details of forward and backward propagation using low-rank tensor network contractions.

### B. Tensorized Linear Layer

We use tensorized linear layers in most computing blocks of a transformer, including the feed-forward networks and the linear transforms in the attention layers.

**Forward propagation.** Most computations in the forward propagation of a transformer involve the matrix-vector product  $\mathbf{y} = \mathbf{W}\mathbf{x}$ , with  $\mathbf{W} \in \mathbb{R}^{M \times N}$  and  $\mathbf{x} \in \mathbb{R}^N$ . Assume that  $M = \prod_{i=1}^d m_i$  and  $N = \prod_{i=1}^d n_i$ , and that  $\mathbf{W}$  is reshaped to a tensor  $\mathcal{W}$  of order  $2d$ . With the TT representation in (6), the matrix-vector product is efficiently computed by low-rank tensor network contraction in our framework. Given the  $2d$  TT cores  $\{\mathcal{G}_k\}_{k=1}^{2d}$  that represent  $\mathbf{W}$ , we compute  $\mathbf{y} = \mathbf{W}\mathbf{x}$  in a tensor-compressed form as

$$y_{i_1, \dots, i_d} = \mathcal{G}_1[i_1] \dots \mathcal{G}_d[i_d] \sum_{j_1, \dots, j_d} \mathcal{G}_{d+1}[j_1] \dots \mathcal{G}_{2d}[j_d] x_{j_1, \dots, j_d} \quad (11)$$

where  $x_{j_1, \dots, j_d}$  and  $y_{i_1, \dots, i_d}$  are elements in the tensor-format input  $\mathcal{X} \in \mathbb{R}^{n_1 \times n_2 \times \dots \times n_d}$  and tensor-format output  $\mathcal{Y} \in \mathbb{R}^{m_1 \times m_2 \times \dots \times m_d}$ , separately. Here  $\mathcal{G}_k[i_k]$  denotes one slice of the order-3 TT core  $\mathcal{G}_k$  by fixing its 2nd index as  $i_k$ . The above equation shows that contraction happens among  $\mathcal{X}$  and the last  $d$  TT cores. Fig. 5(a) shows the graph representation of the above equation when  $d$  is 3. Here, we have an additional free

edge of size  $K$ , because in practice we often perform training with an input dimension  $K$  which is the multiplication of a batch size multiplied with the sequence length. Therefore,  $\mathcal{x}$  should be replaced with a matrix  $\mathbf{X} \in \mathbb{R}^{N \times K}$ .

**Backward propagation.** With low-rank TT parameterization, the BP process for gradient computation can also be done via tensor network contractions. Let us first define the following two tensors:

$$\mathcal{x}' = \frac{\partial \mathcal{L}}{\partial \mathcal{X}}, \quad \mathcal{y}' = \frac{\partial \mathcal{L}}{\partial \mathcal{Y}},$$

which are the order- $d$  tensor representations for  $\mathbf{x}' = \frac{\partial \mathcal{L}}{\partial \mathbf{x}}$  and  $\mathbf{y}' = \frac{\partial \mathcal{L}}{\partial \mathbf{y}}$ , respectively. In standard uncompressed training with  $\mathbf{y} = \mathbf{W}\mathbf{x}$ , it is known that

$$\mathbf{W}' = \frac{\partial \mathcal{L}}{\partial \mathbf{W}} = \mathbf{y}' \mathbf{x}^T.$$

With  $\mathcal{Y}'$  being the high-order tensor representation for  $\mathbf{Y}'$ , the gradient with respect to the TT factors can be computed in two steps:

- We first compute  $\mathcal{X}'$  via a tensor-network contraction

$$x'_{j_1, \dots, j_d} = \mathcal{G}_{2d}^T[j_d] \dots \mathcal{G}_{d+1}^T[j_1] \sum_{i_1, \dots, i_d} \mathcal{G}_d^T[i_d] \dots \mathcal{G}_1^T[i_1] y'_{i_1, \dots, i_d}. \quad (12)$$

- Then the gradients with respect to the  $2d$  TT cores can be computed according to Eq. (9) and Eq. (10) for  $k \in [1, d]$ . Note that  $\mathcal{G}'_k[i_k]$  denotes the  $i_k$ -th slice of the derivative tensor  $\mathcal{G}'_k = \frac{\partial \mathcal{L}}{\partial \mathcal{G}_k}$  by fixing its 2nd index as  $i_k$ .

Fig. 5 (b) and Fig. 5 (c) show the tensor networks of activation gradient and TT core gradients in one linear layer. Note that Fig. 5 (c) illustrates how to compute  $\mathcal{G}'_4$  by eliminating  $\mathcal{G}_4$  from the computing graph. In general, we can remove  $\mathcal{G}_k$  from the tensor network while keeping all other nodes if we want to compute the gradient  $\frac{\partial \mathcal{L}}{\partial \mathcal{G}_k}$ .

### C. Tensorized Embedding Table

The embedding layer in a transformer has huge look-up tables, which consumes a large amount of memory. The TTM



$$\mathcal{F}'_k[i_k, j_k] = \sum_{i_1, \dots, i_{k-1}, i_{k+1}, \dots, i_d} (\mathcal{F}_{k-1}^T[i_{k-1}, j_{k-1}] \dots \mathcal{F}_1^T[i_1, j_1] y'_{i_1, \dots, i_d}) (\mathcal{F}_d^T[i_d, j_d] \dots \mathcal{F}_{k+1}^T[i_{k+1}, j_{k+1}]) \quad (14)$$

$$\text{MUL}_{\text{TT}} = K \sum_{k=0}^{d-1} \left( r_{2d-k-1} r_{2d-k} \prod_{i=1}^{d-k} n_i + r_{d-k-1} r_{d-k} \prod_{i=d-k}^d m_i \right) \quad (15)$$

$$\text{Memory}_{\text{TT}} = Kr_d + K \sum_{k=0}^{d-2} \left( r_{2d-k-1} \prod_{i=1}^{d-k-1} n_i + r_{d-k-1} \prod_{i=d-k}^d m_i \right) \quad (16)$$

$$\text{MUL}_{\text{BTT}} = \sum_{k=0}^{d-2} \left( r_{2d-k-1} r_{2d-k-2} \left( \prod_{i=d-k-1}^d n_i \right) + r_{k+1} r_{k+2} \left( \prod_{i=1}^{k+2} m_i \right) \right) + Kr_d \left( \prod_{i=1}^d m_i + \prod_{i=1}^d n_i \right) \quad (17)$$

$$\text{Memory}_{\text{BTT}} = \sum_{k=0}^{d-2} \left( r_{2d-k-2} \left( \prod_{i=d-k-1}^d n_i \right) + r_{k+1} \left( \prod_{i=1}^{k+2} m_i \right) \right) + Kr_d. \quad (18)$$

representation in (5) can greatly reduce the memory cost of embedding layers, but its forward and backward propagation uses different tensor-network contractions.

**Forward propagation.** Given the  $d$  TTM factors  $\{\mathcal{F}_k\}_{k=1}^d$  that represent  $E_{\text{tok}} \in \mathbb{R}^{M \times N}$ , where  $M = \prod_{i=1}^d m_i$  and  $N = \prod_{i=1}^d n_i$ , and thus  $E_{\text{tok}}$  is reshaped to a tensor  $\mathcal{E}$  of order  $2d$ . In the look-up process, a column of  $E_{\text{tok}}$  is selected for each input token. We use an index vector  $\mathbf{j} = [j_1, j_2, \dots, j_d]$  to select the  $j_k$ -th subtensor of each TTM core  $\mathcal{F}_k$ . The output feature  $y$  could be computed as

$$y_{i_1, \dots, i_d} = \mathcal{F}_1[i_1, j_1] \mathcal{F}_2[i_2, j_2] \dots \mathcal{F}_d[i_d, j_d], \quad (13)$$

where  $\mathcal{F}_k[i_k, j_k]$  is a 2-D slice of  $\mathcal{F}$  by fixing its 2nd and 3rd indices as  $i_k$  and  $j_k$ , respectively. According to the above equation, using the TTM embedding table, we first look up each TTM core using the  $d$ -element index  $\mathbf{j}$ , and use the selected slices to form the output feature.

**Backward propagation.** Since the input index does not require gradients, we only compute the gradients for the tensor cores in the TTM embedding table according to Eq. (14). Here,  $\mathcal{F}'_k[i_k, j_k]$  denotes a slice of the derivative tensor  $\mathcal{F}'_k = \frac{\partial \mathcal{L}}{\partial \mathcal{F}_k}$  by fixing its 2nd and 3rd indices as  $i_k$  and  $j_k$ , respectively.

#### IV. ALGORITHM IMPLEMENTATION

As discussed earlier, forward and backward propagation during tensor-compressed model training is based on tensor contractions. The computation and memory complexity of these operations can vary significantly depending on the order in which the contractions are performed. Existing tensor-compressed inference accelerators typically adopt a right-to-left contraction sequence for both tensor-train matrix (TTM) [39], [41] and TT formats [40]. In this section, we propose an optimized contraction order for the tensor-train (TT)-format linear layer to enhance the performance of our FPGA accelerator.

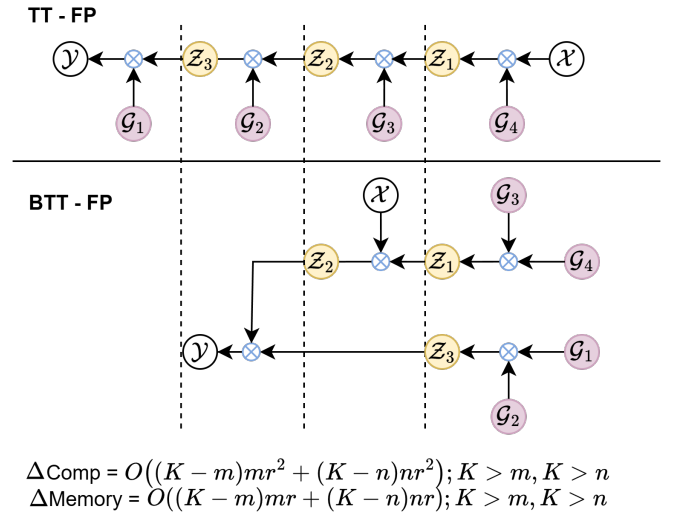


Fig. 6. Comparison of the computing flow of the TT-format and our modified BTT forward propagation for  $d = 2$ . Contraction operations are represented in blue multipliers. Here white nodes represents input tensor  $\mathcal{X}$  and output tensor  $\mathcal{Y}$ ; purple nodes are TT cores  $\mathcal{G}_1$  to  $\mathcal{G}_4$ ; nodes marked in yellow denotes the intermediate contraction results of the involved tensors.

#### A. Complexity of Right-to-Left Contractions

We first evaluate the computational and memory complexity of the right-to-left TT contraction in a linear layer. We only analyze the forward propagation, since computing the gradients with respect to activations and TT cores uses a similar contraction process. The total computational cost in training is roughly  $3\times$  of the inference cost.

**Computational Cost.** The TT-format inference of a linear layer has  $2d$  contraction steps. Generally, the  $k$ -th contraction step (with  $0 \leq k \leq d-1$ ) involves  $Kr_{2d-k-1}r_{2d-k} \prod_{i=1}^{d-k} n_i$  multiplications; the  $(d+k)$ -th step involves  $Kr_{d-k-1}r_{d-k} \prod_{i=d-k}^d m_i$  multiplications. As a re-

TABLE I  
COMPUTATIONAL AND MEMORY COMPLEXITY OF EACH STAGE FOR TTM, RIGHT-TO-LEFT TT CONTRACTION, AND OUR BTT CONTRACTION.

| Cost                                           | Computation                               | Memory                  |                                     |
|------------------------------------------------|-------------------------------------------|-------------------------|-------------------------------------|
|                                                |                                           | Weight                  | Activation                          |
| Matrix multiplication (MM)                     | $O(3Kn^{2d})$                             | $O(n^{2d})$             | 0                                   |
| TTM contraction                                | $O(3Kn^{d+1}((d-2)r^2 + 2r))$             | $O(n^2((d-2)r^2 + 2r))$ | $O(Kn^d(d-1)r)$                     |
| Right-to-left TT contraction                   | $O(6K(\sum_{k=1}^{d-1} n^k r^2 + n^d r))$ | $O(2n((d-2)r^2 + 2r))$  | $O(2K \sum_{k=1}^{d-1} n^k r + Kr)$ |
| Bi-directional TT (BTT) contraction (proposed) | $O(6 \sum_{k=2}^d n^k r^2 + 6Kn^d r)$     |                         | $O(2 \sum_{k=2}^d n^k r + Kr)$      |

sult, the total number of multiplications in a forward pass is estimated in Eq. (15).

**Memory Cost.** Since TT-format training involves multiple contraction steps, additional intra-layer memory costs are required, which is estimated in Eq. (16). Generally, the  $k$ -th contraction step (with  $0 \leq k < d - 1$ ) requires  $Kr_{2d-k-1} \prod_{i=1}^{d-k-1} n_i$  memory cost; the  $(d+k)$ -th step requires  $Kr_{d-k-1} \prod_{i=d-k}^d m_i$  memory. All of these intermediate results need to be stored for reuse in back propagation. As a result, the total number of multiplications in a forward pass is estimated in Eq. (15).

Fig. 6 (top) shows the contraction sequence for a linear layer in TT format when  $d = 2$ . In the right-to-left contraction flow, the computation and memory complexity of every step depend on the input dimension  $K$  which is the batch size multiplied by the sequence length. In NLP and computer vision tasks,  $K$  can be large, leading to low hardware efficiency. To address this limitation, we propose an efficient bidirectional contraction scheme that reduces computational and memory costs by eliminating the dependence on  $K$  in most contraction steps.

### B. Bi-directional Tensor-Train Contraction

Our bidirectional tensor-train (BTT) contraction is shown in Fig. 6 (bottom). Since the left and right  $d$  TT cores have no data dependency, we can perform contraction from the left and right towards the middle in parallel. This can reduce the total number of computation stages from  $2d$  to  $d + 1$ . To better explain the efficiency of the training, we will calculate the exact computation and memory costs for each training stage and compare it with the original right-to-left TT contraction.

Although the total number of contractions (denoted as blue multipliers in Fig. 6) remains unchanged, the computational cost can be significantly reduced by eliminating the dependence on  $K$  in the first  $d - 1$  contraction steps. In the  $k$ -th step, we perform a contraction between a matrix of size  $(\prod_{i=1}^k m_i) \times r_k$  and the TT core  $\mathcal{G}_k \in \mathbb{R}^{r_k \times m_{k+1} \times r_{k+1}}$  on the left, as well as the contraction between the TT core  $\mathcal{G}_{2d-k} \in \mathbb{R}^{r_{2d-k-1} \times n_{d-k} \times r_{2d-k}}$  and a matrix of size  $r_{2d-k} \times \prod_{i=1}^k n_{d-i+1}$  on the right. The resulting total computational cost and memory consumption are estimated as Eq. (17) and Eq. (18). Note that the first terms in both equations are independent of  $K$ . Based on the above equations, BTT always have lower computational complexity when  $m_i$  and  $n_i$  are smaller than  $K$ . This is a common case in modern NLP and computer vision tasks.

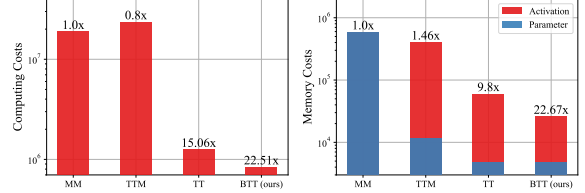


Fig. 7. Comparison of the computation and memory costs of MM, TTM, TT and our modified BTT per linear layer. Hyper-parameter settings are the same as our transformer edge training.

In order to compare our BTT method with other contraction schemes, we summarize the theoretical computing and memory cost of various methods in Table I. The details of TTM complexity are provided in the Appendix VIII. Here we set  $m = n$  to simplify the formulation.

**Example.** We consider a hidden dimension of 768 for the query matrix, and set  $d = 3$  with  $\{n_1, n_2, n_3\}$  and  $\{m_1, m_2, m_3\}$  being  $\{12, 8, 8\}$  and  $\{8, 8, 12\}$ , respectively. We also set the TT rank to 12 and the sequence length to 32. Fig. 7 compares the computation and memory costs of a linear layer implemented with different contraction methods. Clearly, our BTT contraction method consumes the least computation and memory cost. Compared with standard matrix-matrix multiplication, our BTT method is  $22.51 \times$  more computing efficient and  $22.67 \times$  more memory efficient. Compared with the right-to-left TT contraction, our BTT implementation further reduces the computing cost and the memory cost by  $1.49 \times$  and  $2.31 \times$ , respectively.

## V. FPGA ACCELERATOR DESIGN

Based on the new proposed computing scheme, we develop an FPGA accelerator for low-rank tensor-compressed training. We perform hardware-level optimization to further reduce latency and memory usage. We also employ intra-stage and inter-stage dataflow optimization to reduce runtime and memory cost. Our training accelerator is implemented in C++ and transferred to RTL via high-level synthesis (HLS).

### A. Overall Architecture

Fig. 8 (a) shows the overall architecture of our tensor-compressed transformer training accelerator, including tensor-compressed forward propagation (FP) and backward propagation (BP) engines, on-chip and off-chip storage, and data transfer between different training stages. Due to the small

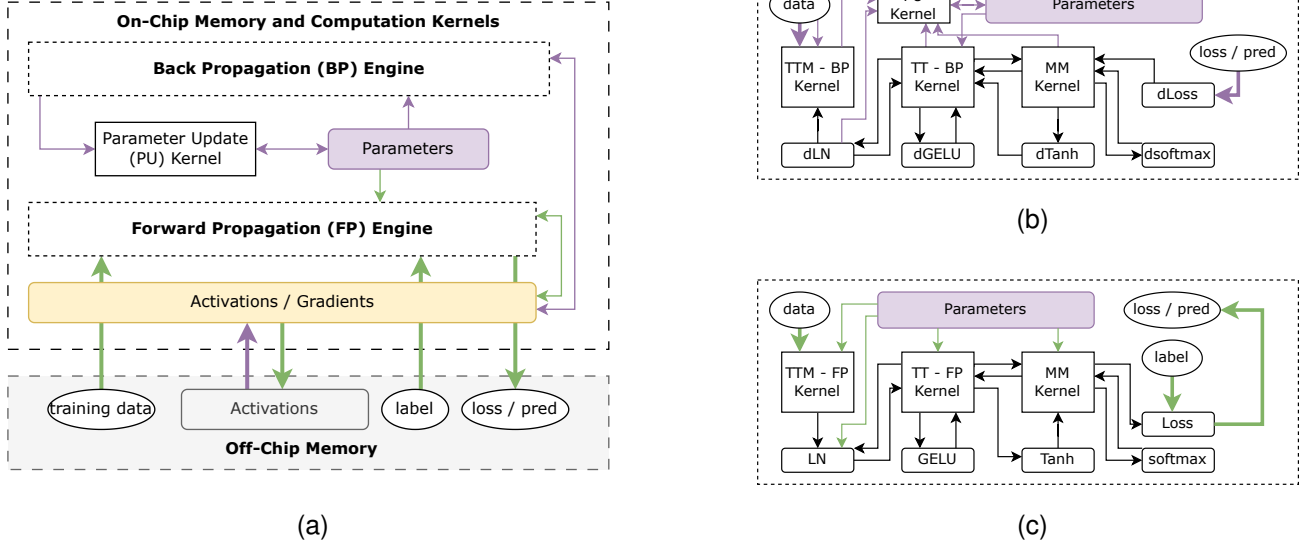


Fig. 8. (a): Overall architecture of the tensorized transformer training accelerator. (b) and (c): The detailed interactions between bottom-level computing kernels during backward and forward propagation. Note that in (b) and (c), the on-chip memory storing activation / gradient interacts with all computing kernels and thus is not shown in the figures.

number of model parameters caused by tensor compression, all training parameters and most activation values are stored in on-chip memory. This reduces the latency and energy overhead caused by off-chip communications. Since the volume of model parameters and activation values increase linearly with the number of layers, the total memory cost still exceeds the on-chip memory budget, thus off-chip memory access is inevitable. We observe that the activation values consume much more memory than the tensor-compressed model parameters. Some interlayer activations produced in FP are needed in BP. To support more complex tasks with more layers, we store these activations in off-chip memory and fetch them to on-chip memory when computing the gradients with respect to tensor factors.

The detailed computing kernels and dataflows inside the tensor-compressed BP and FP engines are shown in Figs. 8 (a) and (b), respectively. To support the whole training progress, multiple computing kernels are developed for various computing schemes, including tensor contraction in the TTM-format embedding table and TT-format linear layers, matrix-multiplication (MM) in the attention parts and classifier, and various non-linear functions (softmax, GELU, Tanh, Layer-Norm) used in transformer models.

### B. Efficient Parallelism for Tensorized Linear Layers

The tensor contraction inside a TT-linear layer is highly sequential. Fortunately, our BTT-linear layer eliminates the data dependency in the first  $d - 1$  contraction steps, which brings parallelism inside the tensor linear layers and reduces the total length of contraction from  $2d$  to  $d + 1$ . However, directly applying intra-layer parallelism without considering inter-layer dataflow will cause inefficient resource usage. We propose task rescheduling and tensor fusion to tackle this problem.

1) *Task Rescheduling for Attention Layers*: Fig. 9 compares the rescheduled parallel BTT and the default scheme for forward propagation of an attention block. Here, we define the contraction kernels as follows:

- **Kernel MUL0**: This kernel denotes the contraction between  $\mathcal{G}_4$  and  $\mathcal{G}_3$  that produces  $\mathcal{Z}_1$ , or the contraction between  $\mathcal{G}_1$  and  $\mathcal{G}_2$  which produces  $\mathcal{Z}_3$ .
- **Kernel MUL1**: this kernel denotes the contraction between the input tensor  $\mathcal{X}$  and the intermediate tensor  $\mathcal{Z}_1$  that produces  $\mathcal{Z}_2$ .
- **Kernel MUL2**: this kernel denotes the contraction between intermediate tensors  $\mathcal{Z}_2$  and  $\mathcal{Z}_3$ , producing the output of a linear layer  $\mathcal{Y}$ . In an attention block,  $\mathcal{Y}$  can be the high-order tensorization of  $\mathbf{Q}$ ,  $\mathbf{K}$  or  $\mathbf{V}$  features.

A naive parallelization (Fig. 9 top right) of the  $\mathbf{Q}$ ,  $\mathbf{K}$  and  $\mathbf{V}$  computation can lead to resource overhead on FPGA. It runs all MUL0 kernels in the linear layers to compute  $\mathbf{Q}$ ,  $\mathbf{K}$  and  $\mathbf{V}$  simultaneously since they are independent. As a result, six MUL0 kernels are needed in total. We use task rescheduling to reduce the hardware cost while achieving the same speedup on FPGA. The optimized tasks scheduling moves non-urgent MUL0 to later time steps and run them with other multipliers in parallel without increasing the total latency. This requires only 2 (rather than 6) reusable computing kernels for MUL0, leading to better resource utilization.

2) *Fused Parallel BTT*: The intermediate results inside a tensor linear layer consume much more memory than the compressed model parameters. Therefore, we propose a fused parallel BTT dataflow to eliminate the memory overhead caused by the intermediate results, as shown in Fig. 10. Here we define the contraction kernels as follows:

- **Kernel MUL2**: this kernel contracts between the output gradient  $\mathcal{Y}'$  and the intermediate result  $\mathcal{Z}_2$ , resulting in  $\mathcal{Z}'_3$ .



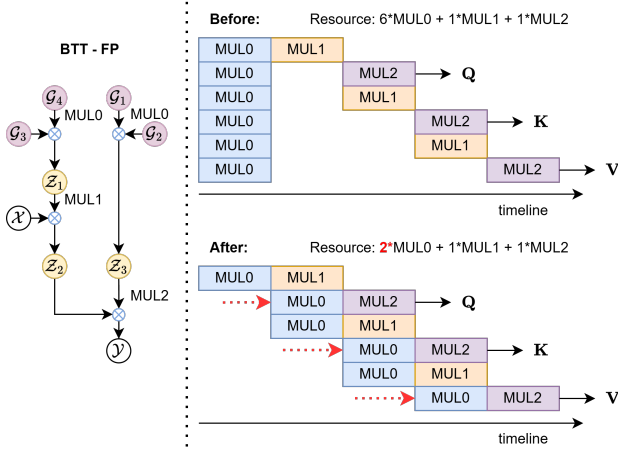


Fig. 9. Schedule viewer of the  $Q$ ,  $K$ ,  $V$  linear layers of BTT-format forward propagation before and after task rescheduling. Left: Purple nodes represent tensor cores, yellow nodes represent intermediate activation, white nodes represent input and output of the TT-linear layer. Right: Different colors represents different tasks.

- **Kernel MUL3:** this kernel contracts the intermediate result  $Z'_3$  and the tensor factor ( $G_1$  or  $G_2$ ), produces  $G'_2$  or  $G'_1$ , respectively, and then performs a parameter update.

We mainly apply operation fusion in these two contraction steps. As denoted in the original scheme (Fig. 10. top), all multiplications for a tensor contraction are completed before the next contraction step. In this way, all intermediate results between contraction steps are required to be stored, which creates a large buffer with high memory consumption. To relieve memory usage, we divide each contraction operation into multiple fine-grained contractions as follows:

- **Fine-Grained Contraction for MUL2:** we perform contraction between sub-tensor  $\mathcal{Y}'[:, i_1, i_2]$  with  $Z_2$  and produce subtensor  $Z'_3[i_1, i_2, :]$ .
- **Fine-Grained Contraction for MUL3:** we perform the contraction between a subtensor  $Z'_3[i_1, i_2, :]$  with another sub-tensor  $G_1[i_1, :]$  (or  $G_2[:, i_2, :]$ ), and produce a result sub-tensor  $G'_2[:, i_2, :]$  (or  $G'_1[i_1, :]$ ).

Here  $i_1 \in \{1, \dots, n_1\}, i_2 \in \{1, \dots, n_2\}$ , and we need to repeat the fine-grained multiplication for  $n_1 n_2$  times. When one fine-grained contraction (Fig. 10 bottom) creates a small intermediate result, the next fine-grained contraction step uses it immediately, and thus only a small buffer with size  $O(r)$  is required for all  $n_1 n_2$  fine-grained contraction steps. The memory cost of intermediate contraction results is completely eliminated in the parameter gradient computation process.

### C. Memory Management on FPGA

While the tensor-compressed training achieves an order-of-magnitude compression ratio in the model parameters, the on-chip memory resources should still be carefully used due to the additional intermediate results required to be stored and reused in training. To address this issue, we reduce on-chip BRAM cost using a TT core grouping method.

Although tensor-compressed training allows storing all model parameters in the BRAM, creating separate memory

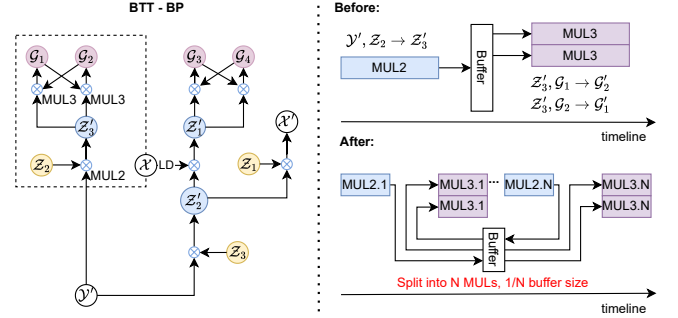


Fig. 10. Schedule viewer of BTT-format back propagation before and after tensor fusion. Left: Purple nodes represent tensor cores, blue nodes represent intermediate activation gradients, yellow nodes represent reused input activation, white nodes represent input and output of the TT-linear layer. Right: Different colors represents different tasks.

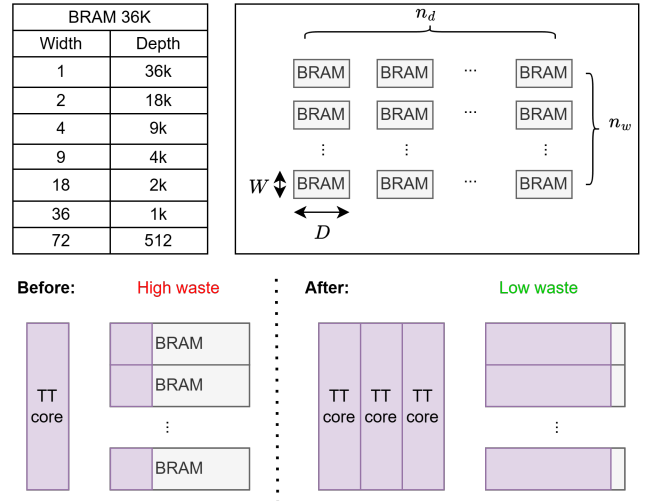


Fig. 11. Configurations of BRAM 36K. Number of BRAM of one array. BRAM usage efficiency before and after tensor grouping.

blocks for multiple small-size TT cores can result in dramatic memory waste because of the fixed BRAM block size on FPGA. We propose a TT core grouping method to improve BRAM utilization.

Each BRAM block in the FPGA has a fixed storage size  $C$ , and can be configured with various widths ( $W$ ) and depths ( $D$ ) with  $C = W \times D$ . For example,  $C = 36,864$  bits for most state-of-the-art AMD FPGA. A BRAM block can be configured as  $W = 1 \sim 72$  as shown in Fig. 11 (top left). In order to store a large data array,  $n_w \times n_d$  BRAM blocks are concatenated in the dimension of “depth” or “width”, as shown in Fig. 11 (top right). Here,  $n_w$  is calculated by the width of the data array divided by  $W$ ,  $n_d$  is calculated by the depth of the data array divided by  $D$ . Both should be rounded up to their nearest integers, respectively. The data array width and depth are decided by the dimensions of the TT core (or grouped TT cores) after it is reshaped into a 2D structure.

To efficiently store the TT cores, we first consider the influence of parallel computing inside each tensor contraction operation. In our design, we implement parallelism over the

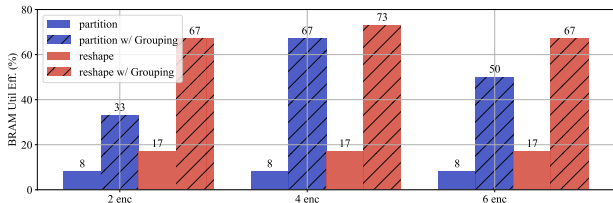


Fig. 12. Comparison of the BRAM utilization efficiency using different memory management strategies in different model sizes.

rank index across all tensor contractions involving TT cores, which requires  $r$  parallel read operations from each TT core. However, since each BRAM block has only two read/write ports, storing an entire TT core in a single BRAM block cannot support parallel access. High-Level Synthesis (HLS) offers two solutions to address this issue. The first approach, known as array partitioning, could partition a large data array into multiple small arrays and map them to separate BRAM blocks. Therefore, we use  $r$  BRAM blocks per TT core to enable parallel data loading. The second approach, known as array reshaping, concatenates multiple elements of the array by increasing the bit-width in order to support parallel data processing. This method is more memory efficient because it only consumes one BRAM block when  $B_w r < \max(W)$ , or  $\lceil \frac{B_w r}{\max(W)} \rceil$  blocks otherwise. In this way, since we use floating-point 32, where  $B_w = 32 (< \max(W) = 72)$ , the required number of BRAM blocks is always smaller than  $r$ .

Assuming that the tensor-compressed transformer involves  $N$  TT cores having the same size for simplicity, the total number of BRAM blocks can be roughly estimated as  $N n_w \times n_d$ . Let  $\lceil x \rceil$  denote rounding up  $x$  to its nearest integer, then  $n_w$  and  $n_d$  can be decided as

$$\text{Array partitioning: } n_w = r \lceil \frac{B_w}{W} \rceil, n_d = \lceil \frac{nr}{D} \rceil, \quad (19)$$

$$\text{Array reshaping: } n_w = \lceil \frac{B_w r}{W} \rceil, n_d = \lceil \frac{nr}{D} \rceil. \quad (20)$$

The above analysis indicates that  $n_d$  will always be 1 since generally  $nr \ll D$ , leading to a huge waste of BRAM resources.

To improve BRAM efficiency, we increase the depth of the array by grouping some TT cores. Specifically, we concatenate  $K$  TT-cores without data dependency into a single array along the depth size, then assign one BRAM block to the whole group. In this case, the total number of BRAM blocks required is  $\frac{N}{K} n_w \times n_d$ , with  $n_w$  and  $n_d$  decided below:

$$\text{Array partitioning: } n_w = r \lceil \frac{B_w}{W} \rceil, n_d = \lceil \frac{Knr}{D} \rceil, \quad (21)$$

$$\text{Array reshaping: } n_w = \lceil \frac{B_w r}{W} \rceil, n_d = \lceil \frac{Knr}{D} \rceil. \quad (22)$$

We can choose  $K$  to make  $\frac{Knr}{D}$  closer to its round-up integer, and thus we can greatly improve the BRAM utilization efficiency, as shown in Fig. 11 (bottom).

The BRAM management problem is formulated as

$$\min_{\theta} F(\theta, \beta) = N n_w n_d, \theta = \{W, D\}, \beta = \{N, K, n, r, B_w\}.$$

TABLE II  
HYPER-PARAMETER SETTINGS OF EACH LAYER IN UNCOMPRESSED AND TENSORIZED TRANSFORMER.

|                | format | matrix shape | tensor shape               | rank |
|----------------|--------|--------------|----------------------------|------|
| embedding      | TTM    | (1000, 768)  | ((10, 10, 10), (12, 8, 8)) | 30   |
| attention      | TT     | (768, 768)   | (12, 8, 8, 8, 8, 12)       | 12   |
| feed-forward   | TT     | (768, 768)   | (12, 8, 8, 8, 8, 12)       | 12   |
| classification | TT     | (768, 768)   | (12, 8, 8, 8, 8, 12)       | 12   |

TABLE III  
PERFORMANCE OF TENSOR-COMPRESSED VERSUS STANDARD MATRIX-FORMAT TRANSFORMER TRAINING ON ATIS DATASET.

| Model        | Intent Acc | Slot Acc | Size (MB)          |
|--------------|------------|----------|--------------------|
| 2-ENC matrix | 96.2%      | 97.3%    | 36.7               |
| 2-ENC tensor | 97.0%      | 97.2%    | <b>1.2 (30.5×)</b> |
| 4-ENC matrix | 95.7%      | 97.4%    | 65.1               |
| 4-ENC tensor | 96.6%      | 97.4%    | <b>1.5 (43.4×)</b> |
| 6-ENC matrix | 96.4%      | 97.5%    | 93.5               |
| 6-ENC tensor | 97.0%      | 97.2%    | <b>1.8 (52.0×)</b> |

With a tensorization setting  $\beta$ , we can find  $W$  and  $D$  to maximize the BRAM utilization according to Eq. (19) – (22).

To show the effectiveness of our method, we define the efficiency of BRAM utilization as  $\eta = \frac{N_{\min}}{N_{\text{total}}}$ , where  $N_{\min}$  is the ideal total memory usage for all tensor factors without considering the capacity of each BRAM block, and  $N_{\text{total}}$  is obtained using our BRAM management scheme. Fig. 12 shows that our BRAM management can achieve a 3.9× to 8.4× higher utilization efficiency than the default memory management.

## VI. EXPERIMENTS

### A. Experimental Setup

We implement our tensor-compressed transformer training accelerator with high-level synthesis (HLS) using C++, and perform synthesis, placement, and routing using Vitis HLS 2023.2 on an AMD Alveo U50 FPGA board. The programmable logic fabric has 872k LUTs, 5952 DSPs, 5.08-MB BRAMs, and 22.5-MB URAMs. All model parameters, activations, and gradients during training are implemented in the floating-point 32-bit (FP32) format with 100-MHz frequency.

We evaluated the FPGA accelerator by training a transformer on the ATIS dataset [50]. This is a data set widely used in natural language understanding (NLU), including audio recordings of customers booking flight tickets. The input sequence length is set to 32, but the accelerator is also reconfigurable to support larger sequence length and for other datasets. For functionality evaluation, we use the stochastic gradient descent (SGD) optimizer with a learning rate  $4 \times 10^{-3}$  and batch size of 1. The hyper-parameters of uncompressed training and our tensor-compressed training are listed in Table II. Table III shows that the tensor-compressed method could achieve the same accuracy with 30.5× to 52.0× compression ratios for transformers with 2 to 6 encoding blocks.

### B. FPGA Accelerator Evaluation

1) *Functionality Evaluation*: To validate the functionality of our transformer training accelerator with parallel BTT

TABLE IV  
RESOURCE UTILIZATION AND POWER CONSUMPTION WITH VARIOUS MODEL STRUCTURE SETTINGS AND INPUT WORKLOAD.

| Model Type | DSP        | LUT        | FF         | BRAM       | URAM      | Power (W) |        |       |
|------------|------------|------------|------------|------------|-----------|-----------|--------|-------|
|            |            |            |            |            |           | Dynamic   | Static | Total |
| 2-ENC      | 2396 (40%) | 565k (65%) | 475k (27%) | 1216 (90%) | 114 (18%) | 20.68     | 6      | 26.68 |
| 4-ENC      | 2396 (40%) | 572k (66%) | 485k (28%) | 1163 (86%) | 128 (20%) | 20.85     | 5.97   | 26.82 |
| 6-ENC      | 2396 (40%) | 579k (67%) | 499k (29%) | 1089 (81%) | 374 (58%) | 20.97     | 6.09   | 27.06 |
| Available  | 5952       | 872k       | 1,743k     | 1344       | 640       | 75        |        |       |

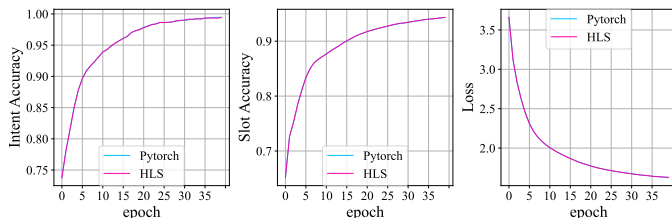


Fig. 13. Training accuracy and loss of the accelerator (2-ENC) compared with PyTorch training in ATIS dataset through the whole training process with 40 epochs.

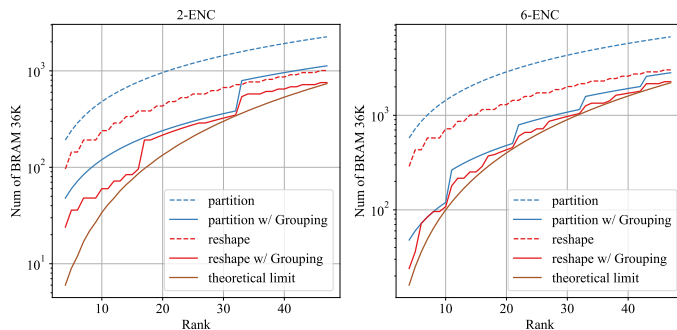


Fig. 14. BRAM usage for all tensor factors using different memory management strategy versus rank

implementation, we compare the training loss and accuracy curves of our high-level synthesis (HLS) FPGA implementation with PyTorch training on a GPU, as illustrated in Fig. 13. The ATIS dataset is a multi-task dataset for both intent classification and slot filling. Intent classification aims to determine the overarching goal or purpose of the user’s query and is treated as a text classification problem. Slot filling identifies key entities or attributes (slots) within a user’s utterance and classifies them into predefined categories. The accuracy and loss curves for both tasks demonstrate that the results from our HLS FPGA implementation closely match those from PyTorch training, confirming the consistency and reliability of our accelerator design.

2) *Effects of BRAM Optimization*: Fig. 14 illustrates the number of BRAMs required to store all TT cores using different allocation methods in Section V-C. It is shown that our proposed BRAM management strategy always consumes the least BRAM resources and even reaches the theoretical limit in some specific rank settings. Our method could bring the actual cost of BRAM closer to the ideal usage, because the TT-core grouping could reduce the waste of depth per BRAM block. Combining this BRAM optimization with tensor

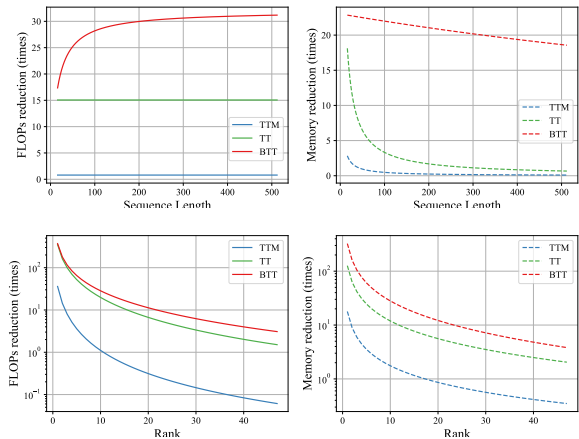


Fig. 15. Computation and memory costs of matrix-matrix multiplication, TTM-based contraction, TT-based contraction and our modified BTT-based contraction per linear layer corresponding to different sequence length (top) and rank (bottom). The reduction ratio is calculated based on matrix-matrix multiplication.

compression, the memory burden is further relieved, allowing storing all compressed model parameters in on-chip memory.

3) *Dependence on TT Ranks and Sequence Length*: To evaluate the influences of the hyper-parameters on our BTT contraction scheme on FPGA, we show the computing and memory costs associated with different sequence length and TT ranks in Fig. 15. The standard matrix-matrix multiplication is used as a baseline to estimate the reduction ratios regarding FLOPs and memory cost. In the upper figure, we fix the TT rank as 12 and increase the sequence length from 8 to 512. In the bottom figure, we fix the sequence length as 32 and increase the TT rank from 1 to 48. As the sequence length increases, our BTT contraction shows greater advantages over the right-to-left contraction of TT and TTM methods in terms of both FLOPs and memory cost. As the TT rank increases, the computing and memory advantage of all tensor-compressed methods degrades, but our BTT scheme always has the highest reduction ratios in both FLOPs and memory costs.

4) *Overall Accelerator Performance*: Table IV presents the hardware resource utilization of our FPGA training accelerator in various model sizes from RTL implementation reports. We evaluated the accelerator with a transformer with 2 to 6 encoder layers. The utilization of DSPs, LUTs, and FFs remains consistent across different model configurations, as the same computational kernels are employed regardless of the model settings. However, BRAM usage decreases while URAM usage increases with a greater number of layers. This

TABLE V  
PERFORMANCE COMPARISON BETWEEN GPU AND OUR FPGA ACCELERATOR.

| Model Settings | Platform-Type | Latency per epoch (second) | Power (W) | Computing Memory |             | Energy per epoch |             |
|----------------|---------------|----------------------------|-----------|------------------|-------------|------------------|-------------|
|                |               |                            |           | (MB)             | Ratio       | (kJ)             | Ratio       |
| 2-ENC          | GPU-matrix    | 47                         | 150       | 829              | <b>48.2</b> | 7.1              | <b>1.38</b> |
|                | GPU-tensor    | 129                        | 141       | 728              | <b>42.3</b> | 18.2             | <b>3.57</b> |
|                | FPGA-tensor   | 191                        | 26.68     | 17.2             | /           | 5.1              | /           |
| 4-ENC          | GPU-matrix    | 77                         | 150       | 915              | <b>51.4</b> | 11.6             | <b>1.29</b> |
|                | GPU-tensor    | 222                        | 141       | 732              | <b>41.1</b> | 31.3             | <b>3.48</b> |
|                | FPGA-tensor   | 335                        | 26.82     | 17.8             | /           | 9.0              | /           |
| 6-ENC          | GPU-matrix    | 108                        | 152       | 1022             | <b>29.6</b> | 16.4             | <b>1.26</b> |
|                | GPU-tensor    | 324                        | 141       | 736              | <b>21.3</b> | 45.7             | <b>3.50</b> |
|                | FPGA-tensor   | 482                        | 27.06     | 34.5             | /           | 13.0             | /           |

behavior can be attributed to the application of our grouping technique to intermediate arrays, which demands additional memory as the number of layers grows. Consequently, HLS automatically allocates these memory requirements to URAM to enhance the utilization efficiency of on-chip memory.

### C. Performance Comparison with GPU

We perform end-to-end performance evaluation of our FPGA accelerator (operating at 100 MHz) compared to the NVIDIA RTX 3090 GPU (acting at 1395 MHz). We compare the memory, latency, power, and energy efficiency on different platforms. For fair comparisons, we measure the whole system-level power of GPU and FPGA.

1) *Memory Cost*: Fig. 16 shows the memory cost of the RTX 3090 GPU and our FPGA accelerator on the ATIS dataset with different model configurations and data formats. For GPU memory, we list two metrics: total memory (extracted from the `nvidia-smi` command) and reserved memory (extracted with the `CUDA memory_reserved` functions). The former measures the memory cost in the entire training process, including the Pytorch back-end overhead. The latter measures only the memory occupied by the model parameters and intermediate variables used in the training. The computing memory of FPGA is the on-chip memory consumption collected from the RTL implementation report. Benefiting from the hardware and algorithm co-design for tensor-compressed training, our FPGA accelerator can perform on-device training with 21.3× to 42.3× lower memory cost compared to tensor-compressed training on GPU. Our optimized on-chip memory management leads to 1.5× to 2.7× memory reduction compared to the reserved memory cost on the GPU.

2) *Energy Cost*: Table V further summarizes the latency per epoch, power consumption, and energy per training epoch of our FPGA accelerator collected from HLS synthesis and RTL implementation reports, compared to both uncompressed training and tensor-compressed training on the GPU. Due to the huge difference in clock frequency, our FPGA accelerator has a higher training latency. However, our FPGA accelerator could achieve around 3.5× lower energy than the tensor-compressed training GPU. We also compare our accelerator with standard matrix-based training on GPU, since GPU is better optimized for standard matrix operations. Due to less back-end overhead, the matrix-format GPU training is more energy efficient than tensor-compressed GPU training.

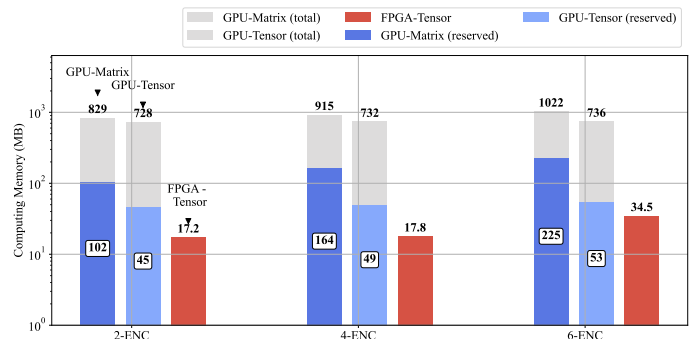


Fig. 16. Comparison of the computing memory costs between GPU (with or without additional overhead) and FPGA in different model size.

However, our FPGA accelerator still achieves around 1.3× lower energy costs while using 29.6× to 51.4× less memory.

3) *Comparison with Previous Work*: Some previous works [57]–[59] achieved higher energy efficiency improvement compared with GPU. However, these works are all CNN training accelerators supporting small models, and their GPU baseline is less powerful than ours. For instance, Ref. [57] using Xilinx ZU19EG FPGA achieved 8.5× improvement in energy efficiency in LeNet-10 compared to the GTX 1080 Ti GPU. However, LeNet-10 has 129× to 328× fewer model parameters and requires 22× to 61× lower total computing costs than our transformer training. Similarly, the work in [59] using Intel Stratix-10 MX FPGA achieved 4.5× higher energy efficiency than Tesla V100 in training the ResNet-20 model. Our transformer model is 41× to 106× larger than ResNet-20, and our computing cost is 6.9× to 18.7× higher. Compared with these results, our accelerator can achieve higher energy efficiency than the more powerful RTX 3090 GPU, and can train much larger models with limited memory.

## VII. LIMITATION AND POTENTIAL IMPROVEMENT

By utilizing tensor-compressed optimization and dedicated hardware design on FPGA, significant improvement has been achieved for transformer training on resource-constrained platforms. However, this work should be considered as a preliminary study of this subject. Based on our observations, there is still potential optimization space worth exploring to further improve the performance of tensor-compressed training from different aspects.

**GPU Performance:** In this work, we implemented tensor-compressed training on GPU using the default PyTorch framework, which leads to significant overhead and under-utilization due to the lack of specialized tensor contraction operators for GPU. Developing fully optimized CUDA kernels for tensor-compressed layers may improve GPU performance and enable greater benefit of tensor compression on GPU platforms. This has been observed in recent work [44].

**FPGA Performance:** The current design uses separate computing kernels for different training stages (forward propagation, backward propagation, parameter update), where resource utilization can be further improved by designing a reconfigurable kernel to exploit kernel reuse. In addition, by increasing the batch size, data parallelism can be utilized to enhance data reuse and improve overall performance.

**Low-Precision Training:** In our current design, the FP32 data format is used as a proof of concept, showing the superiority of the proposed computing scheme and hardware architecture. Recently, many reduced-precision training solutions, such as FP8 [60] and INT8 [61]–[63], have been proposed to accelerate neural network training. By integrating low-precision techniques with our tensor-compressed training framework, the memory and computational complexity can be further reduced. As a result, the overall system-level performance may be further improved.

## VIII. CONCLUSION

In this work, we have developed the first proof-of-concept end-to-end tensor-compressed transformer training accelerator on FPGA. We have identified a key limitation of the prior tensor network accelerators as the low-parallel computing flow and proposed a bidirectional flow with both lower computational costs and memory costs. We have further optimized dataflow and proposed a BRAM memory management method to achieve better latency, memory, and energy efficiency. The proposed tensorized transformer accelerator has achieved up to  $3.6\times$  lower energy costs and  $51\times$  lower computing memory costs than the Nvidia RTX 3090 GPU. The model can scale up to 6 encoder layers and has the potential to solve more complex training tasks on FPGA.

## ACKNOWLEDGMENTS

This work is co-funded by Intel Strategic Research Sectors (SRS) - Systems Integration SRS & Devices SRS.

## APPENDIX

### COMPLEXITY OF TTM CONTRACTION

In the right-to-left contraction flow for TTM-format inference, an input tensor is first contracted with  $\mathcal{F}_d$ , and then  $\mathcal{F}_{d-1}$ , and gradually moves towards the leftmost to finally contract with  $\mathcal{F}_1$  to get the output. The total number of multiplications with  $d$  contraction steps are estimated in Eq. (23). Due to the multiple contraction steps, a TTM-format linear layer creates additional intra-layer activation in each training stage, causing additional memory cost. Additionally, to compute the gradient for each tensor core, all of the intra-layer activation created in the forward pass should be stored

and reused in the backward pass. The overall memory cost is estimated in Equation (24).

$$\text{MUL}_{\text{TTM}} = K \sum_{k=0}^{d-1} r_{d-k-1} r_{d-k} \left( \prod_{i=1}^{d-k} n_i \right) \left( \prod_{i=d-k}^d m_i \right) \quad (23)$$

$$\text{Memory}_{\text{TTM}} = K \sum_{k=0}^{d-2} r_{d-k-1} \left( \prod_{i=1}^{d-k-1} n_i \right) \left( \prod_{i=d-k}^d m_i \right) \quad (24)$$

## REFERENCES

- [1] B. Liu, M. Ding, S. Shaham, W. Rahayu, F. Farokhi, and Z. Lin, "When machine learning meets privacy: A survey and outlook," *ACM Computing Surveys (CSUR)*, vol. 54, no. 2, pp. 1–36, 2021.
- [2] N. Papernot, P. McDaniel, A. Sinha, and M. P. Wellman, "Sok: Security and privacy in machine learning," in *European symposium on security and privacy*, 2018, pp. 399–414.
- [3] K. Wei, J. Li, M. Ding, C. Ma, H. H. Yang, F. Farokhi, S. Jin, T. Q. Quek, and H. V. Poor, "Federated learning with differential privacy: Algorithms and performance analysis," *IEEE transactions on information forensics and security*, vol. 15, pp. 3454–3469, 2020.
- [4] Q. Li, Z. Wen, Z. Wu, S. Hu, N. Wang, Y. Li, X. Liu, and B. He, "A survey on federated learning systems: Vision, hype and reality for data privacy and protection," *IEEE Transactions on Knowledge and Data Engineering*, vol. 35, no. 4, pp. 3347–3366, 2021.
- [5] S. Bansal and C. J. Tomlin, "DeepReach: a deep learning approach to high-dimensional reachability," in *2021 IEEE International Conference on Robotics and Automation (ICRA)*. IEEE, 2021, pp. 1817–1824.
- [6] D. Onken, L. Nurbekyan, X. Li, S. Wu Fung, S. Osher, and L. Ruthotto, "A neural network approach applied to multi-agent optimal control," in *European Control Conference*, 2021.
- [7] D. Sun, S. Jha, and C. Fan, "Learning certified control using contraction metric," in *Conference on Robot Learning*. PMLR, 2021, pp. 1519–1539.
- [8] S. Lee and S. Nirjon, "Learning in the wild: When, how, and what to learn for on-device dataset adaptation," in *Proceedings of the 2nd International Workshop on Challenges in Artificial Intelligence and Machine Learning for Internet of Things*, 2020, pp. 34–40.
- [9] Y. Tang, X. Zhang, P. Zhou, and J. Hu, "EF-train: Enable efficient on-device CNN training on FPGA through data reshaping for online adaptation or personalization," *ACM Transactions on Design Automation of Electronic Systems (TODAES)*, vol. 27, no. 5, pp. 1–36, 2022.
- [10] C. Guo, B. Lou, X. Liu, D. Boland, P. H. Leong, and C. Zhuo, "BOOST: block minifloat-based on-device CNN training accelerator with transfer learning," in *Intl. Conf. Computer Aided Design*, 2023, pp. 1–9.
- [11] J. Lu, C. Ni, and Z. Wang, "ETA: an efficient training accelerator for DNNs based on hardware-algorithm co-optimization," *IEEE Transactions on Neural Networks and Learning Systems*, 2022.
- [12] S. Fox, J. Faraone, D. Boland, K. Vissers, and P. H. Leong, "Training deep neural networks in low-precision with high accuracy using FPGAs," in *Intl. Conf. Field-Programmable Technology*, 2019, pp. 1–9.
- [13] S. Q. Zhang, B. McDaniel, and H. Kung, "FAST: DNN training under variable precision block floating point with stochastic rounding," in *Int. Symp. High-Performance Computer Architecture*, 2022, pp. 846–860.
- [14] A. Vaswani, "Attention is all you need," *Advances in Neural Information Processing Systems*, 2017.
- [15] J. D. M.-W. C. Kenton and L. K. Toutanova, "BERT: Pre-training of deep bidirectional transformers for language understanding," in *Proceedings of naacL-HLT*, vol. 1, 2019, p. 2.
- [16] A. Dosovitskiy, "An image is worth 16x16 words: Transformers for image recognition at scale," *arXiv preprint arXiv:2010.11929*, 2020.
- [17] A. Kirillov, E. Mintun, N. Ravi, H. Mao, C. Rolland, L. Gustafson, T. Xiao, S. Whitehead, A. C. Berg, W.-Y. Lo *et al.*, "Segment anything," in *Proc. CVPR*, 2023, pp. 4015–4026.
- [18] Z. Zhao, X. Ding, and B. A. Prakash, "PINNsFormer: A transformer-based framework for physics-informed neural networks," in *Int. Conf. Learning Representations*, 2024.
- [19] J. Tian, C. Fang, H. Wang, and Z. Wang, "BEBERT: efficient and robust binary ensemble BERT," in *Intl. Conf. Acoustics, Speech and Signal Processing*, 2023, pp. 1–5.
- [20] Y. Ji, C. Fang, and Z. Wang, "BETA: binarized energy-efficient transformer accelerator at the edge," *arXiv preprint arXiv:2401.11851*, 2024.



- [21] N. Wang, J. Choi, D. Brand, C.-Y. Chen, and K. Gopalakrishnan, "Training deep neural networks with 8-bit floating point numbers," in *NIPS*, 2018, pp. 7675–7684.
- [22] Z. Yang, S. Choudhary, S. Kunzmann, and Z. Zhang, "Quantization-aware and tensor-compressed training of transformers for natural language understanding," *arXiv preprint arXiv:2306.01076*, 2023.
- [23] Y. Yang, J. Zhou, N. Wong, and Z. Zhang, "LoRETTA: low-rank economic tensor-train adaptation for ultra-low-parameter fine-tuning of large language models," in *Proc. North American Chapter of the Association for Computational Linguistics: Human Language Technologies*, 2024, pp. 3161–3176.
- [24] C. Fang, A. Zhou, and Z. Wang, "An algorithm–hardware co-optimized framework for accelerating N: M sparse transformers," *IEEE Trans. Very Large Scale Integration Systems*, vol. 30, no. 11, pp. 1573–1586, 2022.
- [25] C. Fang, W. Sun, A. Zhou, and Z. Wang, "Efficient N: M sparse DNN training using algorithm, architecture, and dataflow co-design," *IEEE Trans. CAD of Integrated Circuits and Systems*, 2023.
- [26] W. Wang, F. Wei, L. Dong, H. Bao, N. Yang, and M. Zhou, "MINILM: Deep self-attention distillation for task-agnostic compression of pre-trained transformers," *Advances in Neural Information Processing Systems*, vol. 33, pp. 5776–5788, 2020.
- [27] M. Rhu, M. O'Connor, N. Chatterjee, J. Pool, Y. Kwon, and S. W. Keckler, "Compressing dma engine: Leveraging activation sparsity for training deep neural networks," in *2018 IEEE International Symposium on High Performance Computer Architecture (HPCA)*. IEEE, 2018, pp. 78–91.
- [28] I. Hubara, M. Courbariaux, D. Soudry, R. El-Yaniv, and Y. Bengio, "Quantized neural networks: Training neural networks with low precision weights and activations," *The Journal of Machine Learning Research*, vol. 18, no. 1, pp. 6869–6898, 2017.
- [29] S. Gupta, A. Agrawal, K. Gopalakrishnan, and P. Narayanan, "Deep learning with limited numerical precision," in *International Conference on Machine Learning*, 2015, pp. 1737–1746.
- [30] X. Sun, N. Wang, C.-Y. Chen, J. Ni, A. Agrawal, X. Cui, S. Venkataramani, K. El Maghraoui, V. V. Srinivasan, and K. Gopalakrishnan, "Ultra-low precision 4-bit training of deep neural networks," *NIPS*, vol. 33, 2020.
- [31] T. G. Kolda and B. W. Bader, "Tensor decompositions and applications," *SIAM review*, vol. 51, no. 3, pp. 455–500, 2009.
- [32] V. Lebedev, Y. Ganin, M. Rakhuba, I. Oseledets, and V. Lempitsky, "Speeding-up convolutional neural networks using fine-tuned cp-decomposition," in *3rd International Conference on Learning Representations, ICLR 2015-Conference Track Proceedings*, 2015.
- [33] Y.-D. Kim, E. Park, S. Yoo, T. Choi, L. Yang, and D. Shin, "Compression of deep convolutional neural networks for fast and low power mobile applications," *arXiv preprint arXiv:1511.06530*, 2015.
- [34] P. Zhen, B. Liu, Y. Cheng, H.-B. Chen, and H. Yu, "Fast video facial expression recognition by deeply tensor-compressed LSTM neural network on mobile device," in *Proceedings of the 4th ACM/IEEE Symposium on Edge Computing*, 2019, pp. 298–300.
- [35] F.-H. Meng, Y. Wu, Z. Zhang, and W. D. Lu, "TT-CIM: Tensor train decomposition for neural network in rram-based compute-in-memory systems," *IEEE Trans. Circuits and Systems I: Regular Papers*, 2023.
- [36] R. Guo, Z. Yue, X. Si, T. Hu, H. Li, L. Tang, Y. Wang, L. Liu, M.-F. Chang, Q. Li *et al.*, "15.4 a 5.99-to-691.1 TOPS/W tensor-train in-memory-computing processor using bit-level-sparsity-based optimization and variable-precision quantization," in *2021 IEEE International Solid-State Circuits Conference (ISSCC)*, vol. 64, 2021, pp. 242–244.
- [37] Y. Zhao, X. Xiao, G. Kurczveil, R. G. Beausoleil, and Z. Zhang, "Tensorized optical multimodal fusion network," in *2023 Conference on Lasers and Electro-Optics (CLEO)*. IEEE, 2023, pp. 1–2.
- [38] X. Xiao, M. B. On, T. Van Vaerenbergh, D. Liang, R. G. Beausoleil, and S. Yoo, "Large-scale and energy-efficient tensorized optical neural networks on III–V-on-silicon MOSCAP platform," *APL Photonics*, vol. 6, no. 12, 2021.
- [39] C. Deng, F. Sun, X. Qian, J. Lin, Z. Wang, and B. Yuan, "TIE: energy-efficient tensor train-based inference engine for deep neural network," in *Proc. Int. Symp. Computer Architecture*, 2019, pp. 264–278.
- [40] Y. Gong, M. Yin, L. Huang, J. Xiao, Y. Sui, C. Deng, and B. Yuan, "ETTE: Efficient tensor-train-based computing engine for deep neural networks," in *Proc. Intl. Symp. Computer Architecture*, 2023, pp. 1–13.
- [41] A. Novikov, D. Podoprikin, A. Osokin, and D. P. Petrov, "Tensorizing neural networks," *Advances in neural information processing systems*, vol. 28, 2015.
- [42] G. G. Calvi, A. Moniri, M. Mahfouz, Q. Zhao, and D. P. Mandic, "Compression and interpretability of deep neural networks via Tucker tensor layer," *arXiv:1903.06133*, 2019.
- [43] O. Hrinchuk, V. Khrukov, L. Mirvakhabova, E. Orlova, and I. Oseledets, "Tensorized embedding layers," in *Findings of the Association for Computational Linguistics: EMNLP 2020*, 2020, pp. 4847–4860.
- [44] Z. Yang, Z. Liu, S. Choudhary, X. Xie, C. Gao, S. Kunzmann, and Z. Zhang, "CoMERA: Computing-and memory-efficient training via rank-adaptive tensor optimization," in *Annual Conference on Neural Information Processing Systems*, 2024.
- [45] C. Hawkins, X. Liu, and Z. Zhang, "Towards compact neural networks via end-to-end training: A Bayesian tensor approach with automatic rank determination," *SIAM Journal on Mathematics of Data Science*, vol. 4, no. 1, pp. 46–71, 2022.
- [46] C. Hawkins and Z. Zhang, "Bayesian tensorized neural networks with automatic rank selection," *Neurocomputing*, vol. 453, pp. 172–180, 2021.
- [47] Y. Yang, K. Zhen, E. Banijamal, A. Mouchtaris, and Z. Zhang, "AdaZeta: adaptive zeroth-order tensor-train adaption for memory-efficient large language models fine-tuning," in *Proceedings of the Empirical Methods in Natural Language Processing*, 2024.
- [48] S. Ghiasvand, Y. Yang, Z. Xue, M. Alizadeh, Z. Zhang, and R. Pedarsani, "Communication-efficient and tensorized federated fine-tuning of large language models," *arXiv preprint arXiv:2410.13097*, 2024.
- [49] Y. Zhao, X. Yu, Z. Chen, Z. Liu, S. Liu, and Z. Zhang, "Tensor-compressed back-propagation-free training for (physics-informed) neural networks," *arXiv preprint arXiv:2308.09858*, 2023.
- [50] C. T. Hemphill, J. J. Godfrey, and G. R. Doddington, "The ATIS spoken language systems pilot corpus," in *Workshop on Speech and Natural Language*, 1990.
- [51] I. V. Oseledets, "Tensor-train decomposition," *SIAM Journal on Scientific Computing*, vol. 33, no. 5, pp. 2295–2317, 2011.
- [52] Y. Yang, D. Krompass, and V. Tresp, "Tensor-train recurrent neural networks for video classification," in *International Conference on Machine Learning*. PMLR, 2017, pp. 3891–3900.
- [53] J. Ye, L. Wang, G. Li, D. Chen, S. Zhe, X. Chu, and Z. Xu, "Learning compact recurrent neural networks with block-term tensor decomposition," in *Proc. Computer Vision and Pattern Recognition*, 2018, pp. 9378–9387.
- [54] X. Ma, P. Zhang, S. Zhang, N. Duan, Y. Hou, M. Zhou, and D. Song, "A tensorized transformer for language modeling," *Advances in neural information processing systems*, vol. 32, 2019.
- [55] D. Wang, G. Zhao, G. Li, L. Deng, and Y. Wu, "Compressing 3D CNNs based on tensor train decomposition," *Neural Networks*, vol. 131, pp. 215–230, 2020.
- [56] D. Wang, G. Zhao, H. Chen, Z. Liu, L. Deng, and G. Li, "Nonlinear tensor train format for deep neural network compression," *Neural Networks*, vol. 144, pp. 320–333, 2021.
- [57] Z. Liu, Y. Dou, J. Jiang, Q. Wang, and P. Chow, "An FPGA-based processor for training convolutional neural networks," in *Intl. Conf. on Field Programmable Technology*. IEEE, 2017, pp. 207–210.
- [58] S. K. Venkataramanaiah, Y. Ma, S. Yin, E. Nurvithadhi, A. Dasu, Y. Cao, and J.-S. Seo, "Automatic compiler based FPGA accelerator for CNN training," in *International Conference on Field Programmable Logic and Applications (FPL)*. IEEE, 2019, pp. 166–172.
- [59] S. K. Venkataramanaiah, H.-S. Suh, S. Yin, E. Nurvitadhi, A. Dasu, Y. Cao, and J.-s. Seo, "FPGA-based low-batch training accelerator for modern CNNs featuring high bandwidth memory," in *Proc. International Conference on Computer-Aided Design*, 2020, pp. 1–8.
- [60] J. Lu, J. Huang, and Z. Wang, "THETA: A high-efficiency training accelerator for DNNs with triple-side sparsity exploration," *IEEE Transactions on Very Large Scale Integration (VLSI) Systems*, vol. 30, no. 8, pp. 1034–1046, 2022.
- [61] J. Lu, J. Lin, and Z. Wang, "A reconfigurable dnn training accelerator on FPGA," in *2020 IEEE Workshop on Signal Processing Systems (SiPS)*. IEEE, 2020, pp. 1–6.
- [62] H. Shao, J. Lu, J. Lin, and Z. Wang, "An FPGA-based reconfigurable accelerator for low-bit DNN training," in *2021 IEEE Computer Society Annual Symposium on VLSI (ISVLSI)*. IEEE, 2021, pp. 254–259.
- [63] M. Wang, S. Rasoulizhad, P. H. Leong, and H. K.-H. So, "NITI: Training integer neural networks using integer-only arithmetic," *IEEE Transactions on Parallel and Distributed Systems*, vol. 33, no. 11, pp. 3249–3261, 2022.